AIAA 80-1428R

Numerical Treatment of Unsteady Subsonic Flow Past an Oscillating Cascade

Joseph R. Caspar* and Joseph M. Verdon*
United Technologies Research Center, East Hartford, Conn.

A numerical procedure for determining unsteady subsonic flow past a finite-deflection, oscillating cascade is described. Based on the assumption of small-amplitude blade motions, the unsteady flow is governed by linear equations with variable coefficients which depend on the underlying steady flow. These equations are solved on a nonorthogonal, body-fitted, and periodic grid which facilitates the implementation of blade, wake, and cascade-periodicity conditions but disallows the use of standard difference approximations. Instead, difference approximations are based on an implicit least-squares development applicable on arbitrary grids. This permits flexibility in the choice of difference neighbors and the simultaneous approximations of differential equation and boundary conditions at boundary points, strategies which can significantly improve numerical accuracy. Sample results illustrating the effects of blade thickness, motion frequency, and inlet Mach number on the unsteady response of staggered cascades are presented.

Introduction

An unsteady aerodynamic analysis which accounts for the effects of mean flow deflection due to blade geometry and flow turning and is capable of providing efficient predictions of unsteady response coefficients is an important requirement for turbomachinery applications. A general aerodynamic model which fully includes the effects of nonuniform mean or steady flow on a small-disturbance unsteady flow has been formulated and described in Refs. 1 and 2. The steady flow is governed by the full potential equations, and the unsteady flow is governed by linear equations with variable coefficients which depend on the underlying steady flow. In contrast to classical linear theory, an unsteady aerodynamic formulation which includes the effects of nonuniform mean flow requires numerical solutions of the governing steady and unsteady boundary value problems. Numerical procedures for determining steady subsonic[3] or transonic[4] potential flow through cascades are currently available. A solution procedure for the linear, variable-coefficient, unsteady problem is described in the present paper.

Since the unsteady aerodynamic model treats realistic cascade configurations, the numerical approximation must take into account nonrectangular geometries. Generally, approximations to differential equations in nonrectangular regions are developed in one of two ways. A mapping may be defined so that in mapped variables calculation points can be placed in a rectangular grid; the transformed equations are then approximated using rectangular difference expressions in the usual way. Alternatively, more general difference approximations may be defined so that differential equations can be approximated on nonrectangular meshes in physical variables. Thompson, Thames, and Mastin[5] have defined global mappings for arbitrary two-dimensional bodies, but these mappings are inappropriate for cascades since the resulting meshes generally do not allow for cascade periodicity. Ives and Liutermoza[4] have determined global mappings which transform infinite two-dimensional cascade regions into rectangular computational regions while allowing for cascade periodicity. However, the necessary mappings are not presently known for all cascades, particularly those with high turnings or small gap-to-chord ratios, and the method cannot be extended to three dimensions. Jameson and Caughy[6] have employed a local mapping concept in which a nonorthogonal grid is constructed in physical space. The local mesh around each grid point is then mapped to a rectangular box where the locally transformed equation is approximated. This "finite-volume" approach has the advantage of general applicability in two- or three-dimensional space but requires computation of nonphysical quantities. Caspar, Hobbs, and Davis[3] employ a control area approach for approximating the steady, two-dimensional, full potential equation expressed in conservation form on a nonorthogonal grid in the physical plane. Although this method avoids the necessity of a mapping step and can be extended to three dimensions, it is limited in that it cannot be applied to equations in general (i.e., nonconservative) form.

In the present paper a straightforward method for approximating general differential equations in nonrectangular regions in physical space is developed and applied to the small-disturbance unsteady cascade problem. Differential quantities are approximated at a point in terms of function values at neighboring points using an interpolation in an implicit manner. The choices of interpolation and neighbors are very flexible, giving rise to a general family of approximating methods. The particular interpolation used here is a least-squares quadratic fit and the neighbors come from an easily defined, nonorthogonal, periodic mesh. The interpolation is modified at boundaries to permit, in effect, the simultaneous approximation of field equation and boundary condition, and the choice of neighbors is adjusted near blade edges to avoid differencing across singularities, strategies which significantly improve accuracy. Although this approach is applied here to a linear, variable-coefficient, two-dimensional problem, it can be readily extended to treat nonlinear problems of arbitrary dimension.

The Unsteady Aerodynamic Model

The aerodynamic model has been derived in detail in Refs. 1 and 2 and will only be summarized here. In the following discussion, all quantities are dimensionless. Lengths have been scaled with respect to blade chord, time with respect to the ratio of blade chord to upstream freestream speed, and pressure with respect to the upstream freestream dynamic pressure. Isentropic and irrotational flow of a perfect gas past a two-dimensional, subsonic cascade is considered (Fig. 1). The blades of the cascade have finite thickness, camber, and mean incidence relative to the inlet flow and are undergoing identical, small-amplitude, harmonic motions at frequency ω and constant interblade phase angle σ. Only rigid blade

Presented as Paper 80-1428 at the AIAA 13th Fluid and Plasma Dynamics Conference, Snowmass, Colo., July 14-16, 1980; submitted Aug. 20, 1980; revision received May 28, 1981.

*Principal Scientist. Member AIAA.

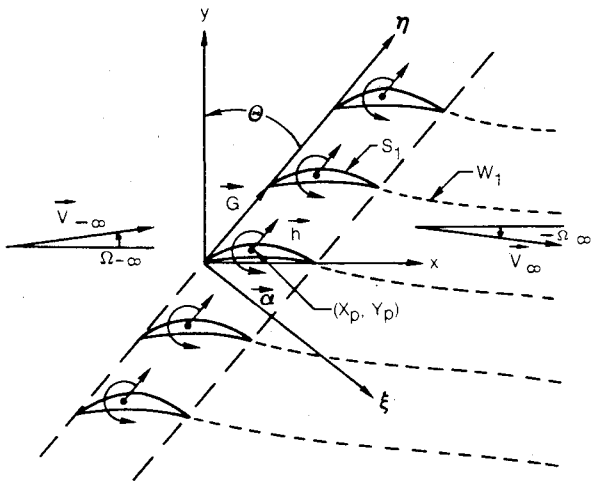

Fig. 1 Two-dimensional oscillating cascade with finite mean flow deflection.

motions are considered, and thus the relative displacement vector for the mth blade, $m=0,\pm1,\pm2,\ldots$, is given by

$$\mathfrak{R}_m = re^{i(\omega t+m\sigma)} = (\boldsymbol{h}+\boldsymbol{\alpha}\times\boldsymbol{R}_p)e^{i(\omega t+m\sigma)} \tag{1}$$

where t is time, $\boldsymbol{h}$ defines the amplitude and direction of blade translations, $\boldsymbol{\alpha}$ is an out-of-plane vector whose modulus α defines the amplitude of blade rotations, and $\boldsymbol{R}_p$ is a vector extending from the mean position of the mth axis of rotation to points on the mean position of the mth blade surface S_m. The components h_x, h_y, and α of the vectors $\boldsymbol{h}$ and $\boldsymbol{\alpha}$ are in general complex to permit phase differences between the translations in the x and y directions and the rotation.

Blade shape and orientation relative to the stream and the amplitude and frequency of the blade motion are assumed to be such that the flow remains attached to the blade surfaces (i.e., the flow tangency condition applies). In addition, the fluid pressure and normal velocity are continuous across the blade wakes. In the inviscid approximation the wakes are represented by thin vortex sheets, each of which emanates from a point in the vicinity of a blade trailing edge and extends downstream. The mean positions W_m of the unsteady wakes are assumed to coincide with the steady flow rear stagnation streamlines. In the far field the flow consists of unsteady fluctuations, due to outward acoustic wave propagation and vorticity convection (downstream), about uniform inlet and exit conditions.

The Unsteady Boundary Value Problem

The velocity potential $\hat{\Phi}(X,t)$ is expanded in an asymptotic series in a small parameter ϵ, i.e.,

$$\hat{\Phi}(X,t) = \sum_{j=0}^{\infty} \epsilon^j \phi_j(X,t) = \Phi(X) + \phi(X)e^{i\omega t} + 0(\epsilon^2) \tag{2}$$

where X is a position vector. In addition Taylor series expansions are used to refer boundary conditions to the mean positions of the blade and wake surfaces. After substituting these series into the full governing equations, equating terms with like powers in ϵ, and neglecting terms of second and higher order in ϵ, nonlinear and linear variable-coefficient boundary value problems are obtained, respectively, for the zeroth- and first-order potentials.[1,2]

The zeroth-order potential describes steady flow past a stationary cascade and is assumed to be known in the present study (cf, Refs. 3 and 4). The cascade geometry, the prescribed form of the blade motion, and the linearity of the first-order equations require that the first-order or unsteady potential be harmonic in time, i.e., $\epsilon\phi_1(X,t)=\phi(X)e^{i\omega t}$, and that the first-order, unsteady flow exhibit blade-to-blade periodicity, i.e., $\phi(\xi,\eta+G)=\phi(\xi,\eta)e^{i\sigma}$, where G is the blade spacing and ξ and η are axial and tangential Cartesian coordinates, respectively (see Fig. 1). These conditions permit a time-independent, boundary value problem for the unsteady potential to be formulated for a single, extended blade passage region of the cascade.

Within this region the unsteady potential, $\phi(X)$, is governed by a linear differential equation of the form

$$\mathfrak{L}_0\phi \equiv \sum_{\nu=0}^{5} c^\nu D^\nu \phi = 0 \tag{3}$$

where the differential operators D^ν are defined by

$$\begin{aligned} &D^0\phi=\phi, \quad D^1\phi=\phi_\xi, \quad D^2\phi=\phi_\eta \\ &D^3\phi=\phi_{\xi\xi}, \quad D^4\phi=\phi_{\xi\eta}, \quad D^5\phi=\phi_{\eta\eta} \end{aligned} \tag{4}$$

and the coefficients c^ν are variable and depend on the underlying steady flow, i.e.,

$$\begin{aligned} c^0 &= \omega^2 - i\omega(\gamma-1)\nabla^2\Phi \\ c^1 &= -[2i\omega+(\gamma-1)\nabla^2\Phi]\Phi_\xi - 2\nabla\Phi\cdot\nabla\Phi_\xi \\ c^2 &= -[2i\omega+(\gamma-1)\nabla^2\Phi]\Phi_\eta - 2\nabla\Phi\cdot\nabla\Phi_\eta \\ c^3 &= A^2-\Phi_\xi^2, \quad c^4 = -2\Phi_\xi\Phi_\eta, \quad c^5 = A^2-\Phi_\eta^2 \end{aligned} \tag{5}$$

Here γ is the specific heat ratio of the fluid and A is the local speed of sound in the steady flow.

The unsteady potential is subject to the following conditions on the upper and lower boundaries of the extended blade passage region. On blade surfaces the flow tangency condition requires that

$$\mathfrak{L}_1\phi \equiv \nabla\phi\cdot n - [i\omega r + \alpha\times\nabla\Phi - (r\cdot\nabla)\nabla\Phi]\cdot n e^{im\sigma} = 0 \tag{6}$$

Across wake surfaces, the condition of continuity of pressure and normal velocity require

$$\mathfrak{L}_\nu\phi^- - \mathfrak{L}_\nu\phi^+ = 0, \qquad \nu=2,3 \tag{7}$$

where

$$\mathfrak{L}_2\phi \equiv i\omega\phi + \nabla\Phi\cdot\nabla\phi \qquad \mathfrak{L}_3\phi \equiv \nabla\phi\cdot n \tag{8}$$

and the superscripts + and − refer to positions on the upper and lower sides of the wake, respectively.

In general unsteady disturbances do not attenuate in the far field, as do steady disturbances, and, hence, it is difficult to place explicit conditions on the unsteady potential on upstream and downstream boundaries of the extended blade passage region. Instead, analytic solutions have been determined by assuming that the steady velocity V is uniform in the far field. These solutions can be matched to the nearfield numerical solution at finite distances upstream and downstream of the blade row.

The unsteady potential is continuous far upstream of the blade row (i.e., $\phi=\phi_c$ for $\xi\le\xi_-$) and has both continuous and discontinuous components far downstream of the blade row (i.e., $\phi=\phi_c+\phi_d$ for $\xi\ge\xi_+$). The continuous potential accounts for acoustic wave propagation into the far field and can be determined by Fourier methods as[1,2]

$$\phi_c(\xi,\eta) = \sum_{j=-\infty}^{\infty} b_{j,\mp}\exp(iq_j\eta)\exp[\chi_{j,\mp}(\xi-\xi_\mp)]$$

$$\mp\xi \ge |\xi_\mp| \tag{9}$$

where the coefficients $b_{j,\mp}$ are obtained from the relation

$$b_{j,\mp} = G^{-1} \int_{\eta}^{\eta+G} \phi_c(\xi,\eta) \exp(-iq_j\eta)\, d\eta, \quad \xi = \xi_{\mp} \tag{10}$$

The discontinuous component of the potential results from countervorticity shed from blade trailing edges and convected along the wakes. A closed-form solution for this potential has been obtained,[1] i.e.,

$$\phi_d(\tau,v) = \Delta\phi(\xi_+,\eta_+) F(v) \exp(-i\omega\tau/V_\infty), \quad \xi \geq \xi_+ \tag{11}$$

in terms of the Cartesian coordinates τ and v with the τ axis coinciding with the mean position of the far downstream, zeroth (or reference) wake and directed downstream. Here $\Delta\phi$ is the difference in ϕ across the reference wake, i.e., $\Delta\phi = \phi^- - \phi^+$, and (ξ_+,η_+) is the point of intersection of this wake and the far downstream boundary. The constants q_j, $\chi_{j,\pm}$, and the function $F(v)$ in the foregoing equations are defined explicitly in Ref. 2.

Aerodynamic Response Coefficients

A solution to the unsteady boundary value problem is required to determine unsteady surface-pressure distributions and aerodynamic force and moment coefficients. It follows from Bernoulli's equation and the isentropic relations that the unsteady pressure $p_{\$} e^{i(\omega t + m\sigma)}$, acting on moving blade surfaces $\$_m$, is determined from

$$\begin{aligned} p_{\$} &= -2(M_{-\infty}A)^{2/(\gamma-1)} [i\omega\phi + \nabla\Phi\cdot\nabla\phi \\ &\quad + (r\cdot\nabla)\,|\,\nabla\Phi\,|^{\,2}/2]_s \\ &= [-2(M_{-\infty}A)^{2/(\gamma-1)} (i\omega\phi + \nabla\Phi\cdot\nabla\phi) + r\cdot\nabla P]_s \end{aligned} \tag{12}$$

where $M_{-\infty}$ is the upstream freestream Mach number, P is the steady pressure, and the right-hand side is evaluated at the mean position of the reference blade. Unsteady force and moment coefficients, $\boldsymbol{c}_F e^{i(\omega t+m\sigma)}$ and $c_M e^{i(\omega t+m\sigma)}$, respectively, are determined by simple integrations over the mean position of the reference blade, i.e.,

$$\boldsymbol{c}_F = -\oint_s p_{\$} \boldsymbol{n}\, ds + \boldsymbol{\alpha}\times\boldsymbol{c}_F \qquad c_M = \oint_s p_{\$} \boldsymbol{R}_p \cdot \mathbf{ds} \tag{13}$$

where $\boldsymbol{c}_F$ is the steady force coefficient and $\mathbf{ds}$ is the differential vector tangent to the mean blade surface. Force components are positive when acting in the positive coordinate directions, and moments are positive when acting in the counterclockwise direction.

The Numerical Model

In the approximate representation of a physical problem by a discrete numerical model, several components must be constructed. For the present case, these components include the discrete domain (or calculation mesh), the approximating algebraic equations, and the solution procedure. Such components are generally not independent of each other with the choice of one influencing the choice of another. For instance, if the algebraic system is linear with proper structure, a direct solution procedure may be used; but if the system is nonlinear or linear but large and without particular structure, an iterative technique may be necessary. It is important that the choice of one component not place overly restrictive constraints on the other components.

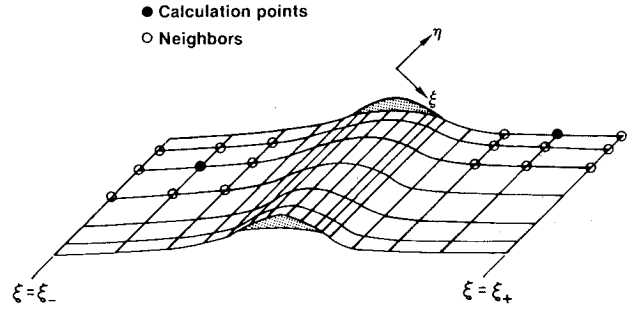

Fig. 2 Unsteady calculation mesh.

The Calculation Mesh

Cascade periodicity makes the definition of an appropriate calculation mesh more difficult for cascades than for isolated airfoils. For the latter there are potential-streamline meshes, "polar" meshes composed of normal and circumferential lines, and "parabolic" combinations. For a cascade these meshes are not so easily employed. For instance, the potential-streamline mesh is not periodic since potential lines generally are not parallel to the cascade. Boundary conditions arising from cascade periodicity—in this case the periodic and wake boundary conditions—can be approximated on such a mesh only with difficulty, since the mismatch of the mesh across the periodic boundary will require some sort of interpolation. In addition, the resulting linear system will not be tightly banded, precluding the use of direct solution techniques. Furthermore, a suitable mesh for this analysis should have the upstream and downstream boundaries parallel to the cascade direction to simplify the application of the far-field matching conditions.

The mesh used in the present analysis is the periodic and body-fitted but nonorthogonal one shown schematically in Fig. 2. It is composed of "axial" lines parallel to the cascade direction and "tangential" curves which are percentile averages of the lower and upper passage boundaries. This mesh is easily defined and conforms properly to all boundaries. Using a skewing transformation, a mesh such as that of Fig. 2 could easily be mapped into a rectangular mesh on which transformed differential equations would be approximated with the usual rectangular difference approximations based on Taylor series expansions. However, the nonorthogonality of the mesh in the physical plane caused by blade shape and especially by cascade stagger may cause loss of accuracy of the resulting difference equations. This is because the importance of neighboring points is not optimally assigned as the mesh deviates from orthogonal. The approach followed in this paper avoids mapping and uses instead a general approximation method applicable on general discrete sets of points. The method automatically assigns proper importance to neighboring points.

Algebraic Approximations

Consider a linear differential operator $\mathcal{L}$ which operates on a constant by multiplying that constant by q^0. $\mathcal{L}\phi$ is to be approximated at the mesh point Q_0 in terms of the values of ϕ at Q_0 and at certain neighboring mesh points, $Q_1,\ldots,Q_M$, which, with Q_0, are called a neighbor set. Neighbor sets are defined as shown in Fig. 2, i.e., in a "centered" fashion for points in the stream and in a "one-sided" fashion for points on a blade or wake boundary. Quantities subscripted with 0 or m are evaluated at the corresponding neighbor set member. The approximation is developed in terms of an implicit interpolation of the form

$$\delta\phi \equiv \phi - \phi_0 \approx F = \sum_{n=1}^{N} \gamma^n f^n \equiv f^T\boldsymbol{\gamma} \tag{14}$$

where the f^n are prescribed interpolating functions which vanish at Q_0 (homogeneous polynomials, for instance) and the γ^n are interpolating coefficients which depend on local values of ϕ and are determined by the specific interpolation used. An algebraic approximation to $(\mathcal{L}\phi)_0 = \mathcal{L}\phi(Q_0)$ is then simply obtained by replacing ϕ with $\phi_0 + F$, i.e.,

$$(\mathcal{L}\phi)_0 \approx \mathcal{L}(\phi_0 + F)_0 = q^0\phi_0 + (\mathcal{L}f)_0^T\gamma \tag{15}$$

where $\mathcal{L}f$ is the $N\times 1$ vector with components $\mathcal{L}f^n$.

For the present application the interpolating functions are chosen to be the polynomials

$$N=5:\ f^1=\delta\xi,\ f^2=\delta\eta,\ f^3=\delta\xi^2,\ f^4=\delta\xi\cdot\delta\eta,\ f^5=\delta\eta^2 \tag{16}$$

where $\delta\xi = \xi - \xi_0$, $\delta\xi^2 = (\xi-\xi_0)^2$, etc. The interpolation coefficients must then be defined. With eight neighbors but only five interpolating functions, it is impossible to define γ such that F implicitly agrees with $\delta\phi$ at all neighbors. On a rectangular mesh the reasonable but ad hoc decisions that F agree with $\delta\phi$ at the neighbors above, below, right, and left and that a certain combination of F values at the corner neighbors agree with the same combination of $\delta\phi$ values would produce the familiar rectangular mesh difference approximations. On a general mesh these ad hoc decisions are no longer reasonable. What is needed is a formal method for defining the interpolating coefficients from the available data regardless of the geometry of the neighbor set. Least-squares techniques provide such a method.

A measure of the error in replacing $\delta\phi$ with its interpolate F in Eq. (14) is

$$e(\gamma) \equiv \sum_{m=1}^{M} w_m \Big[\sum_{n=1}^{N}\gamma^n f_m^n - \delta\phi_m\Big]\overline{\Big[\sum_{n=1}^{N}\gamma^n f_m^n - \delta\phi_m\Big]} \tag{17}$$

where the overbar indicates complex conjugation and the w_m are chosen to give proper importance to the various neighbors. In practice w_m is usually given by

$$w_m = 1/|\,Q_m - Q_0\,| \tag{18}$$

but it may be set to zero if the corresponding neighbor is to have no influence. Note that since ϕ is complex and the f^n are real, the γ^n must be complex. The error function is minimized by setting its derivatives with respect to the real and imaginary parts of the γ^n equal to zero. There results the complex linear system

$$\sum_{n=1}^{N}\Big(\sum_{m=1}^{M} w_m f_m^n \bar{f}_m^k\Big)\gamma^n = \sum_{m=1}^{M} w_m \bar{f}_m^k \delta\phi_m;\ k=1,\ldots,N \tag{19}$$

which can be written in compact form as

$$\mathfrak{A}\gamma = \mathfrak{B}\delta\phi \tag{20}$$

The $N\times N$ matrix $\mathfrak{A}$ and the $N\times M$ matrix $\mathfrak{B}$ are given in terms of the $M\times N$ matrix $\mathfrak{F} = (f_m^k)$ and the $M\times M$ diagonal matrix, $W = \text{diagonal}\,(w_1,\ldots,w_m)$ by

$$\mathfrak{A} = \mathfrak{F}^* w \mathfrak{F} \qquad \mathfrak{B} = \mathfrak{F}^* w \tag{21}$$

where the superscript * indicates conjugate transposition. Thus,

$$\gamma = (\mathfrak{A}^{-1}\mathfrak{B})\delta\phi \equiv \mathfrak{C}\delta\phi \tag{22}$$

where $\mathfrak{C}$ is an $N\times M$ matrix. By combining Eqs. (15) and (22), the approximating difference operator can be defined in terms of local values of ϕ by

$$(\mathcal{L}\phi)_0 \approx (L\phi)_0 \equiv q^0\phi_0 + (\mathcal{L}f)_0^T\mathfrak{C}\delta\phi$$

$$= q^0\phi_0 + \sum_{m=1}^{M}\beta_m(\phi_m - \phi_0) \tag{23}$$

where the difference coefficients are given by

$$\beta^T = (\beta_1,\ldots,\beta_M) \equiv (\mathcal{L}f)_0^T\mathfrak{C} \tag{24}$$

For the least-squares definition of the difference weights to be possible, the matrix $\mathfrak{A}$ of Eq. (21) must be nonsingular, i.e., the rank of $\mathfrak{A}$ must be N. Since the rank of $\mathfrak{A}$ is equal to the rank of $\mathfrak{F}$ which is at most M, the number of neighbors (M) must be at least as large as the number of interpolating functions (N). This however, is not sufficient. Singularity of $\mathfrak{A}$ is equivalent to the existence of a nontrivial $N\times 1$ vector $\boldsymbol{b}$ for which $\mathfrak{F}\boldsymbol{b} = \mathbf{0}$, i.e., for which the equation

$$\sum_{n=1}^{N} b^n f^n(Q) = 0 \tag{25}$$

is satisfied at Q_0 and all its neighbors. If the f^n are the polynomials [Eqs. (16)], the solution sets of Eq. (25) are quadratic curves. Thus care must be taken that Q_0 and its neighbors do not all lie on a quadratic curve (or two straight lines).

Since the difference approximation of Eq. (23) arises from the implicit use of an interpolation, which, in this case, uses least-squares techniques, it is termed generally an implicit interpolation approximation and specifically an implicit least-squares approximation.

Modifications to the Interpolation

The interpolation of Eq. (14) is defined by three components: the set of interpolating functions, the neighbor set (on which the interpolating functions are sampled), and the interpolation rule. If any of these components is altered, a different interpolation and hence a different difference operator is obtained. Thus the implicit interpolation method is actually a family of approximating methods. Various modifications are now discussed.

Derivatives of the unsteady potential exhibit singular behavior at sharp blade edges, in that $\phi \sim (r^{1/2})$ near leading edges and $\phi \sim (r^{3/2})$ near trailing edges where r denotes distance from the edge.[7] To avoid taking differences across singularities, either the first point(s) on the blade or the first point off the blade on the lower and upper boundaries can be deleted from neighbor sets near the blade edges. Affected neighbor sets are said to be adjusted. This modification has been found to improve accuracy as demonstrated by the discussion of Fig. 3 below. The edge singular behavior could perhaps also be treated by modifying the set of interpolating functions to include appropriate singular functions; however, this approach has not been tried.

For each of the first-order boundary operators of Eqs. (6) and (8), the direct application of the above procedure results in a difference operator which is diagonally weak in that the coefficient of ϕ_0 (the diagonal term) is small compared to the sum of the absolute values of the off-diagonal terms. The diagonal weakness may be a symptom of the fact that not all available information is being employed when the boundary condition alone is approximated. Specifically, the field equation of Eq. (3) also holds at boundary points. This information can be integrated into the difference equation by employing a "boundary constraint" modification to the interpolation rule in which the interpolate, $\phi_0 + F$, is constrained to satisfy Eq. (3) at Q_0. Thus the interpolating coefficients γ^n are determined by minimizing the error function e, not over the space of all quadratic polynomials but rather only over the subset of quadratics which satisfy the

following constraint on γ:

$$0=\mathcal{L}_0(\phi_0+F)_0=q_0^0\phi_0+(\mathcal{L}_0 f)_0^T\gamma$$

$$=q_0^0\phi_0+\sum_{n=1}^{N}\gamma^n(\mathcal{L}_0 f^n)_0\equiv g(\gamma) \tag{26}$$

The interpolating coefficients are then determined by seeking an extremum of the constraint function

$$e_c(\gamma,\lambda)=e(\gamma)+\mathrm{Re}(\lambda)\,\mathrm{Re}(g(\gamma))+\mathrm{Im}(\lambda)\,\mathrm{Im}(g(\gamma)) \tag{27}$$

as the real and imaginary parts of γ and the Lagrange multiplier λ are varied. The resulting linear system, which replaces that of Eq. (20) is

$$\mathcal{A}\gamma+(\overline{\mathcal{L}_0 f})_0\lambda=\mathcal{B}\delta\phi \qquad (\mathcal{L}_0 f)_0^T\gamma=-q_0^0\phi_0 \tag{28}$$

with solution (the value of λ is unimportant)

$$\gamma=\mathcal{C}_c\delta\phi-b_c q_0^0\phi_0 \tag{29}$$

where

$$b_c=\mathcal{A}^{-1}(\overline{\mathcal{L}_0 f})_0/[(\mathcal{L}_0 f)_0^T\mathcal{A}^{-1}(\overline{\mathcal{L}_0 f})_0]$$
$$\mathcal{C}_c=\mathcal{C}-b_c(\mathcal{L}_0 f)_0^T\mathcal{C} \tag{30}$$

After substituting Eqs. (29) and (30) into Eq. (15), Eq. (23) becomes

$$(\mathcal{L}\phi)_0\approx(L_c\phi)_0\equiv(L\phi)_0-s(L_0\phi)_0 \tag{31}$$

where L and L_0 are the difference operators arising from unconstrained approximations to $\mathcal{L}$ and $\mathcal{L}_0$, respectively, and s is the scalar

$$s=(\mathcal{L}f)_0^T b_c=(\mathcal{L}f)_0^T\mathcal{A}^{-1}(\overline{\mathcal{L}_0 f})_0/[(\mathcal{L}_0 f)_0^T\mathcal{A}^{-1}(\overline{\mathcal{L}_0 f})_0] \tag{32}$$

Thus the constrained difference operator on the boundary is a particular linear combination of the field and unconstrained boundary difference operators. It has been found to be much stronger diagonally and to provide generally more accurate results as indicated by the discussion of Fig. 4 below.

Comparisons with Standard Rectangular Approximations

On a rectangular mesh the commonly used rectangular difference approximations to the Laplacian operator is the familiar five-point formula involving the center point and the points above, below, right, and left which form a rectangular cross. The implicit least-squares approximation with all eight neighbors in the neighbor set involves all neighbors and so differs from the five-point formula. However, if two opposing corner points are deleted from the neighbor set, the difference coefficients corresponding to the other two corner points vanish and the five-point formula is obtained. Furthermore, if the mesh is then skewed so that the opposing corner points in the neighbor set form a rectangular cross with the center point and the points above and below, the five-point formula is automatically recovered but now with the difference coefficients of the displaced right and left points vanishing. This does not happen when a skewing transformation is used. Thus the implicit least-squares approximation automatically adjusts to mesh nonorthogonality to give proper importance to the neighbors.

The Linear System and Solution Procedure

At field points the unsteady differential equation [Eq. (3)] is approximated using centered neighbor sets. For points on the upstream upper periodic boundary, ϕ values at neighbors above the mesh region are related to ϕ values at points within the mesh region by cascade periodicity, while on the upstream lower periodic boundary periodicity is directly applied. For points on the far upstream boundary, ϕ values at neighbors upstream of the mesh region are related to ϕ values on the boundary using the far-field condition [Eq. (9)] with the Fourier coefficients being evaluated using Eq. (10). The infinite sum in Eq. (9) is truncated after a few terms (usually three) in each direction, and the integral in Eq. (10) is approximated using a trapezoid rule quadrature. A similar procedure is followed on the far downstream boundary, but here the discontinuous component of ϕ given in Eq. (11) must also be taken into account. At blade points the flow tangency condition [Eq. (6)] is approximated using one-sided neighbor sets. At wake points the pressure continuity and normal velocity operators of Eqs. (8) are also approximated using one-sided neighbor sets. Letting L_U and L_L represent either one of the approximating difference operators on the upper and lower wakes, respectively, the resulting difference equations take the form

$$L_U\phi(Q_U)-e^{i\sigma}L_L\phi(Q_L)=0 \tag{33}$$

where Q_L is a mesh point on the lower wake and Q_U is the corresponding point on the upper wake. Continuity of pressure is applied on one wake boundary and continuity of normal velocity is applied on the other wake boundary. Because of the stabilizing effects of neighbor set adjustment and boundary constraint, the former is always used near the blade edges and the latter is always used on the blade and wake boundaries.

There are I axial mesh lines ordered from upstream to downstream and J tangential mesh curves ordered from lower to upper boundary. Let ϕ_i be a vector of ϕ values on the ith axial mesh line. Because the mesh is periodic and neighbor sets for points on the ith line include points only from lines $i-1$, i, and $i+1$, the system of linear algebraic equations described above has block tridiagonal form, i.e.,

$$B_1\phi_1+C_1\phi_2=d_1$$
$$A_i\phi_{i-1}+B_i\phi_i+C_i\phi_{i+1}=d_i,\quad 2\le i\le I-1 \tag{34}$$
$$A_I\phi_{I-1}+B_I\phi_I=d_I$$

where the submatrices A_i, B_i, and C_i are $J\times J$ and sparse, being essentially scalar tridiagonal. With this structure, the system can be solved directly and efficiently using Gaussian elimination as described in Refs. 8 and 9. The sparsity of the submatrices can be taken advantage of to improve computational efficiency during the forward elimination phase of the solution.[9] If a nonperiodic mesh were employed the block tridiagonal structure would be lost and an iterative solution procedure would be required.

Numerical Results

The cascade mesh of Fig. 2 is not suitable for the accurate description of unsteady flow properties near blunt edges. Thus results are shown here only for cascades for which the near edge flow can be reasonably approximated on such a mesh, i.e., for cascades of sharp-edged blades with mean camber lines aligned with the steady flow. Procedures for resolving the local unsteady flow near blunt edges are under development and will be reported in the future.

The standard mesh used for examples in this paper has 15 tangential mesh lines and 69 axial mesh lines, 25 of which intersect blade surfaces. The calculation domain extends from two axial chord lengths upstream of the leading edge to two axial chord lengths downstream of the trailing edge. The spacing of the axial mesh lines as a percentage of axial chord varies from 2% near blade edges to 5% near midchord, while the spacing of the tangential mesh lines as a percentage of

distance between the lower and upper boundaries varies from 2% near the boundaries to 15% near the middle of the blade passage. To minimize the effect of local errors spilling into the global solution, axial mesh lines have been chosen not to intersect blade leading and trailing edges.

Numerical results for flat-plate cascades and unstaggered cascades of thin- and double-circular-arc blades have been reported in Ref. 2. Those for flat-plate cascades were shown to be in very good agreement with Smith's[10] classical linear theory predictions for both subresonant and super-resonant blade motions. Predictions for unstaggered cascades of double-circular-arc and thin-circular-arc blades have revealed that blade thickness has a significant effect on unsteady response while the effect of flow turning due solely to blade camber is only minimal. In this paper selected results for staggered cascades of flat-plate and double-circular-arc blades are presented first to demonstrate the capabilities of the numerical approximation (in particular, the salutory effects of neighbor set adjustment and boundary constraint) and then to illustrate partially the effects of blade thickness, inlet Mach number, and motion frequency on unsteady response.

The reference blade surface is defined by the equation

$$y(x) = \pm F(x) = \pm\,[T/2 - R + \sqrt{R^2 - (x-0.5)^2}],$$

$$0 \le x \le 1;\quad R = (T^2+1)/4T \qquad (35)$$

where R is the radius of curvature and T the thickness of the profile. Unsteady pressure difference distributions (i.e., $\Delta p = p[x,y^-(x)] - p[x,y^+(x)]$) will be presented for cascades undergoing single-degree-of-freedom heaving motions [with $h_y = (1,0)$] or pitching motions with $\alpha = (1,0)$ about an axis at midchord, $(X_p,\ Y_p) = (0.5,\ 0)$. These rigid, two-dimensional motions model bending or torsional vibrations of actual rotor blades. When the imaginary parts of the bending or torsional amplitudes are set equal to zero, the real and imaginary parts of the response coefficients Δp, c_L, and c_M are in phase with the blade displacement and velocity, respectively. The stability of single-degree-of-freedom bending motions for real h_y is governed by the sign of the imaginary part of the lift coefficient. If $\mathrm{Im}\{c_L\} < 0$ the airstream resists the motion, and hence this motion is stable according to linear theory. Similarly, if α is real, single-degree-of-freedom torsional motions are stable when $\mathrm{Im}\{c_M\} < 0$.[11]

Except where noted the unsteady results reported here were obtained using the standard mesh. Steady flows were calculated on a different but similar mesh using the finite-area approximation of Ref. 3 and interpolated to the unsteady mesh using constrained, polynomial, least-squares interpolations in an explicit manner. To avoid conditions which lead to flow separation at blade edges, inlet ($\Omega_{-\infty}$) and exit (Ω_∞) flow angles (Fig. 1) have been determined by using steady-flow Kutta conditions, i.e.,

$$\boldsymbol{V}\cdot\mathbf{ds}\Big|_{s^-} = -\,\boldsymbol{V}\cdot\mathbf{ds}\Big|_{s^+} \qquad (36)$$

at both leading and trailing edges.

Effects of Adjusting and Constraining

Edge singularities, particularly the stronger ones at leading edges, pose difficulties for any finite-difference calculation. However, neighbor set adjustment to avoid differencing over singularities can drastically improve results. This is seen in Fig. 3 which shows the unsteady pressure difference distributions calculated using the standard mesh with and without adjusted neighbor sets near the edges. This case involves uniform steady flow through a staggered cascade of oscillating flat plates (a classical linear theory example) at conditions indicated in the figure. The leading-edge singularity causes a severe distortion of the pressure profile

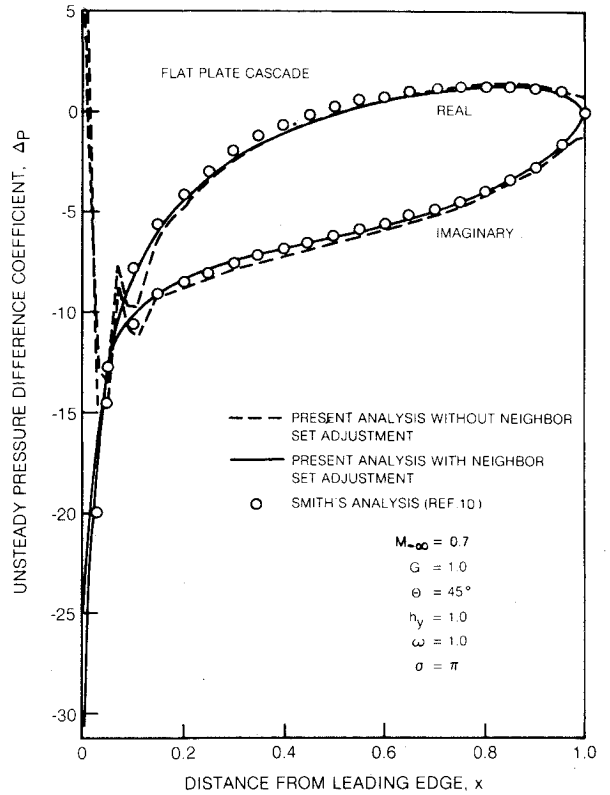

Fig. 3 Alleviation of singularity problems by neighbor set adjustment.

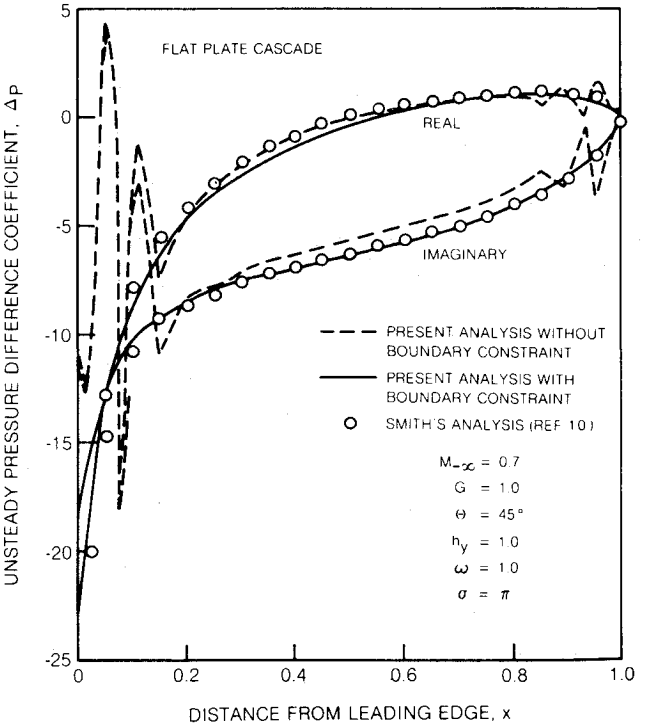

Fig. 4 Alleviation of mesh aspect problems by constraining.

calculated with unadjusted neighbor sets. The distortion is significant only over the first 15% or so of blade chord, but on a finer mesh the singularity has greater influence and the distortion becomes more extensive. The weaker singularity at the trailing edge has the effect only of preventing pressure closure which must occur for this case. By contrast, the pressure difference distribution calculated with adjusted neighbor sets is not significantly distorted by either the leading- or trailing-edge singularity, and it is in good

agreement with Smith's[10] semianalytical prediction except that it does not show a true singularity at the leading edge.

Although the use of neighbor set adjustment prevents differencing across edge singularities, locally strong gradients can still cause problems, particularly if the mesh spacing in one direction is much greater than that in the other. Use of a boundary constraint to a great extent eliminates such mesh aspect ratio problems. This is seen in Fig. 4 which shows constrained and unconstrained calculated pressure difference distributions for the same case as in Fig. 3 with adjusted neighbor sets, but on a mesh with a finer ξ spacing and a coarser η spacing than that of the standard mesh. The oscillations at leading and trailing edges in the unconstrained result are absent from the constrained prediction which agrees well with that of Smith.

Parametric Study

Blade Thickness

Unsteady pressure difference distributions for out-of-phase ($\sigma=\pi$), single-degree-of-freedom bending ($h_y=1$) and torsional ($\alpha=1$) vibrations are shown in Figs. 5 and 6, respectively, for staggered cascades of flat-plate ($T=0$) 10% thick ($T=0.1$) and 20% thick ($T=0.2$) airfoils. The motions occur at unit frequency ($\omega=1$) and at an inlet Mach number $M_{-\infty}$ of 0.5. Steady inlet and exit flow angles are as follows: for $T=0$, $\Omega_{\mp\infty}=0$ deg; for $T=0.1$, $\Omega_{\mp\infty}=2.1$ deg; and for $T=0.2$, $\Omega_{\mp\infty}=4.5$ deg. The results shown in Figs. 5 and 6 reveal a significant coupling between the steady and the first-order unsteady flows due to blade thickness. Both out-of-phase bending and torsional vibrations are stable for the three cascade configurations. However, the imaginary components of the pressure difference distributions indicate that the effect of increasing blade thickness is stabilizing for bending motions ($\mathrm{Im}\{c_L\}$ decreases as T increases) and destabilizing for out-of-phase torsional motions ($\mathrm{Im}\{c_M\}$ increases as T increases).

Except in the vicinity of blade edges, the variations in unsteady loading due to increasing blade thickness, depicted in Figs. 5 and 6, are primarily caused by variations in the steady and unsteady velocities tangent to the blade surface [cf, Eq. (12)], particularly the latter. However, for the 20% thick airfoil, relatively large steady velocity or pressure gradients occur and these cause real unsteady pressure differences due to out-of-phase bending to be less than those for the 10% thick profile (Fig. 5). In addition, large steady gradients cause rapid variations in the real component of the unsteady pressure near the edges of thick blades. The numerical results for thick profiles do not indicate pressure closure (i.e., $\mathrm{Re}\{\Delta p\}\neq 0$) at trailing edges because the relative displacement term ($r\cdot\nabla P$) does not have the same value on upper and lower surfaces of wedge-shaped trailing edges.

Inlet Mach Number

The effect of inlet Mach number $M_{-\infty}$ on the unsteady response to 10% thick double-circular-arc blades undergoing unit frequency bending oscillations is illustrated in Figs. 7 and 8. Steady inlet and exit flow angles for these cases are as follows: for $M_{-\infty}=0.3$, $\Omega_{\mp\infty}=1.9$ deg; for $M_{-\infty}=0.5$, $\Omega_{\mp\infty}=2.1$ deg; for $M_{-\infty}=0.7$, $\Omega_{\mp\infty}=2.6$ deg. Results similar to those shown in Fig. 7 have also been obtained for flat-plate cascades (with $\Omega_{\mp\infty}=0$). Changes in the real and imaginary pressure difference distributions for out-of-phase bending motions of flat-plate cascades are relatively small, but such motions do become more stable ($\mathrm{Im}\{c_L\}$ decreases) with increasing Mach number. In contrast, pressure difference distributions for 10% thick double-circular-arc blades show large variations and a substantial increase in stability margin as Mach number is increased. Differences between the aerodynamic response to out-of-phase bending motions of flat-plate and 10% thick double-circular-arc blade cascades are greater at $M_{-\infty}=0.7$, indicating that the coupling between steady and unsteady flows due to blade thickness is particularly strong at high Mach number.

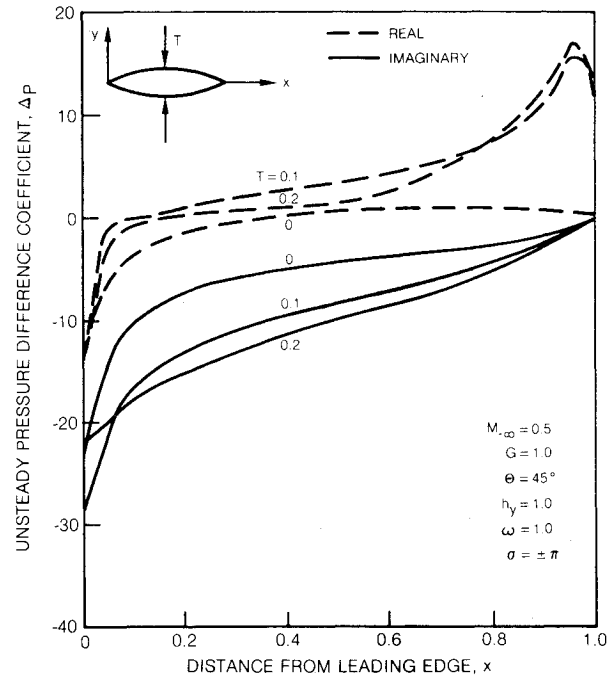

Fig. 5 Effect of thickness on unsteady response due to bending vibrations.

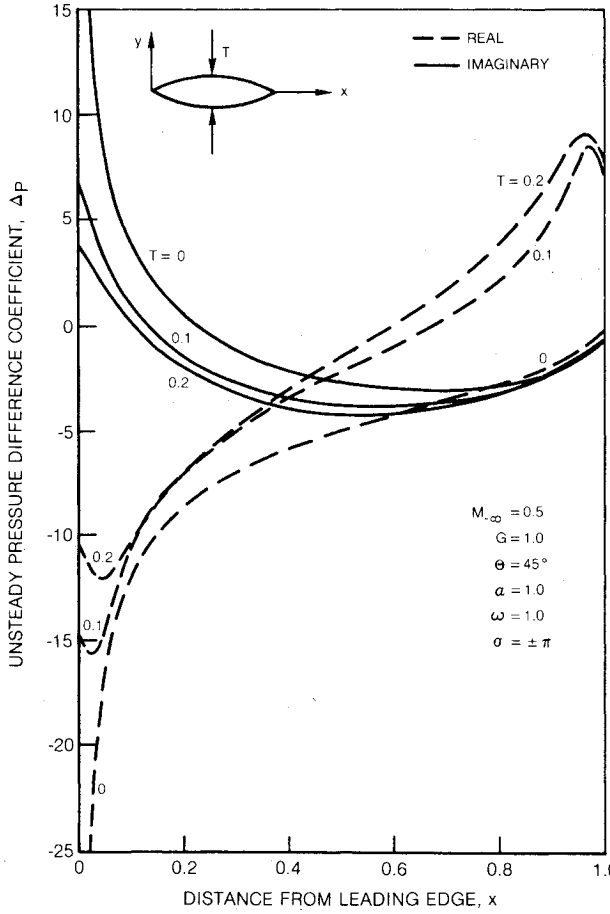

Fig. 6 Effect of thickness on unsteady response due to torsional vibrations.

Results for unit frequency, in-phase, bending vibrations are shown in Fig. 8. There are substantial changes in both real and imaginary components of the unsteady loading as inlet Mach number is increased from low or moderate values ($M_{-\infty}=0.3$ or 0.5) to a relatively high value ($M_{-\infty}=0.7$). These are primarily due to variations in the imaginary component of the unsteady potential, which affects real

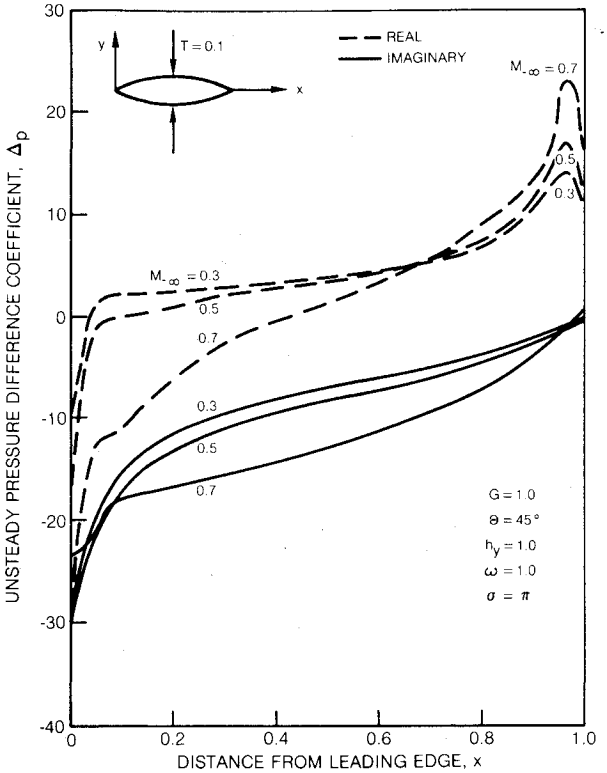

Fig. 7 Effect of Mach number on unsteady response due to out-of-phase bending vibrations.

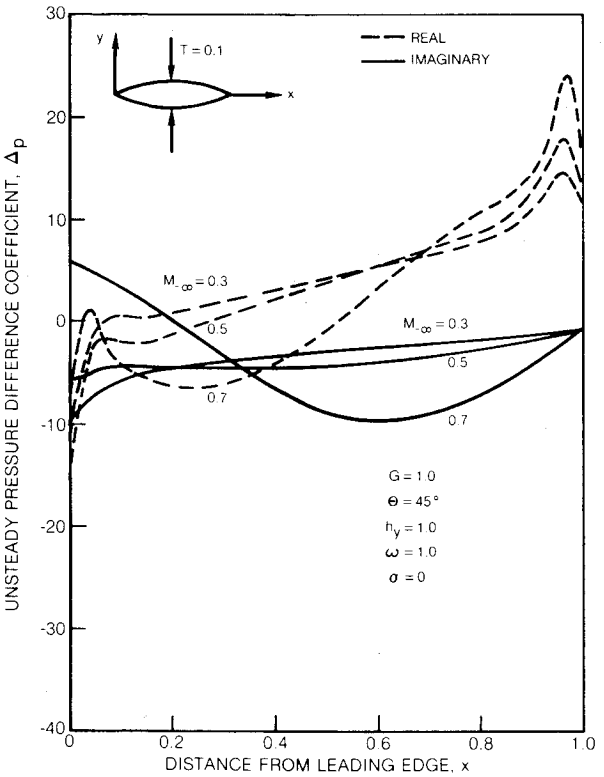

Fig. 8 Effect of Mach number on unsteady response due to in-phase bending vibrations.

unsteady pressures through the local time derivative term $\omega \mathrm{Im}\{\phi\}$ and imaginary unsteady pressures through the velocity product term $\nabla\Phi \cdot \mathrm{Im}\{\nabla\phi\}$. Numerical results for in-phase bending vibrations of flat-plate cascades (not shown) indicate that Mach number variation has an insignificant effect on unsteady response. In contrast, inlet Mach number variations have a substantial impact on the aerodynamic

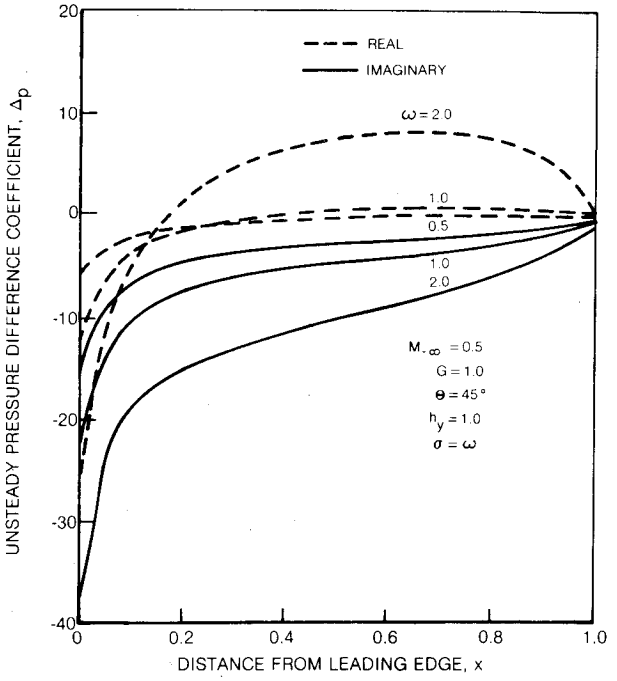

Fig. 9 Effect of frequency on unsteady response due to out-of-phase bending vibrations for a flat-plate cascade.

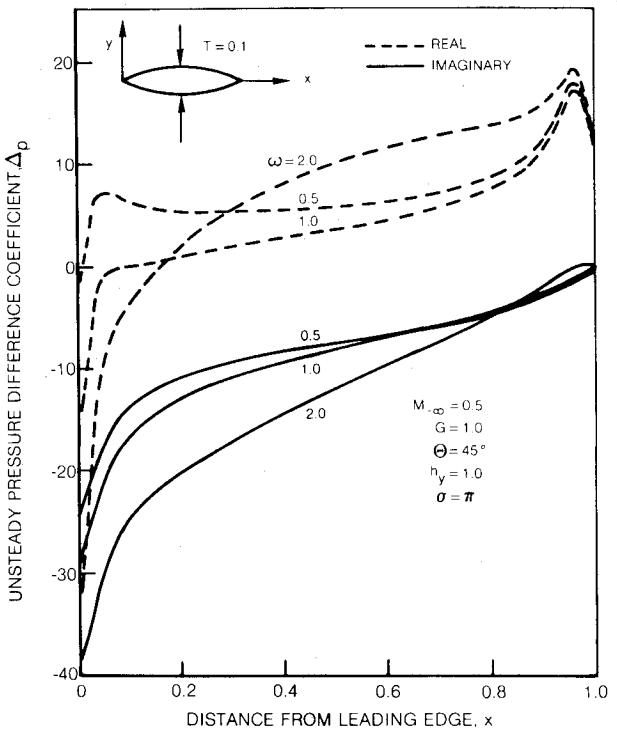

Fig. 10 Effect of frequency on unsteady response due to out-of-phase bending motions for a cascade of double-circular-arc airfoils.

response to in-phase bending motions of thick blades, particularly at high Mach number. Unsteady lift coefficients for the cases studied in Fig. 8 reveal that the stability of in-phase bending vibrations is enhanced as Mach number is increased.

Frequency

Results for out-of-phase bending oscillations at $\omega = 0.5$, 1.0, and 2.0 of flat-plate and 10% thick double-circular-arc blades are shown in Figs. 9 and 10, respectively. Here the inlet Mach number is 0.5, and the inlet and exit steady flow angles are 0 deg for the flat-plate cases and 2.1 deg for the double-circular-arc cases. The effect of increasing frequency is

strongly stabilizing for out-of-phase bending motions of flat-plate (Fig. 9) and 10% thick double-circular-arc (Fig. 10) profiles. For low ($\omega = 0.5$) and moderate ($\omega = 1.0$) frequencies the stability margin is substantially greater for the thick profiles than it is for the flat-plate blades, while at the high frequency ($\omega = 2.0$) profile thickness produces a much smaller increase in the magnitude of the force opposing the blade motion. The velocity product $\nabla\Phi \cdot \nabla\phi$ provides the dominant contribution to the loading at low to moderate frequencies, while at high frequency the local time derivative term $i\omega\phi$ provides the major contribution to the loading except near the blade edges.

Conclusion

Aerodynamic and numerical models have been developed to determine unsteady flow past a finite-deflection, subsonic oscillating cascade. The aerodynamic model assumes small-amplitude fluctuations about a nonuniform steady flow and accounts for the effects of blade geometry and steady flow turning on unsteady response. The unsteady potential satisfies a linear differential boundary value problem with variable coefficients defined by the steady flow. Thus the unsteady flow is coupled to the nonlinear steady flow—a feature not included in classical linear aerodynamic theory.

The numerical model is general and comprehensive enough to approximate accurately the unsteady equations despite the difficulties posed by cascade periodicity and nonrectangular geometry. The approach followed avoids mapping by approximating differential quantities in the physical plane using finite differences defined with an implicit interpolation. The approximation is flexible enough to be applied on a general placement of calculation points so that it can be applied on a nonrectangular mesh, and neighbor sets can be adjusted to avoid differencing across singularities—an important feature for this problem. Furthermore, both differential equation and boundary condition can, in effect, be simultaneously approximated at boundary points. This significantly improves accuracy in areas where local mesh aspect ratios are abnormally large or small. The implicit interpolation is a linear combination of polynomials with the coefficients determined by a weighted least-squares procedure. However, more general interpolations involving more general function combinations can be used. Although applied to the linear aerodynamic model, the implicit interpolation procedure can easily be applied to nonlinear problems as well. Thus it has great flexibility to handle complex problems with complex geometries.

Unsteady response predictions have been presented for simple cascade configurations consisting of sharp-edged blades aligned with the mean flow. For such cases, the unsteady flow in the blade edge regions can be reasonably approximated on a relatively coarse "global" mesh. Numerical procedures employing local reanalysis and solution matching concepts to treat general blade profiles and mean incidence are under current development. Numerical results presented here and in Ref. 2 indicate that blade thickness produces strong steady-unsteady interactions, particularly at high Mach number. In addition, for single-degree-of-freedom blade motions, it appears that the effects of increasing thickness, Mach number, and frequency are stabilizing for bending vibrations, while increasing thickness may be destabilizing for torsional vibrations. However, due to the large number of parameters entering the problem, it is difficult to establish definitive trends in unsteady response without extensive parametric studies.

Acknowledgment

This research was sponsored in part by the Commercial Products Division, Pratt & Whitney Aircraft Group, United Technologies Corporation.

References

[1] Verdon, J. M., Adamczyk, J. J., and Caspar, J. R., "Subsonic Flow Past an Oscillating Cascade with Unsteady Blade Loading - Basic Formulation," *Unsteady Aerodynamics,* edited by R. B. Kinney, Vol. 2, March 1975, pp. 827-851.

[2] Verdon, J. M. and Caspar, J. R., "Subsonic Flow Past an Oscillating Cascade with Finite Mean Flow Deflection," *AIAA Journal,* Vol. 18, May 1980, pp. 540-548.

[3] Caspar, J. R., Hobbs, D. E., and Davis, R. L., "Calculation of Two-Dimensional Potential Cascade Flow Using Finite Area Methods," *AIAA Journal,* Vol. 18, Jan. 1980, pp. 103-109.

[4] Ives, D. C. and Liutermoza, J. F., "Second Order Accurate Calculation of Transonic Flow Over Turbomachinery Cascades," *AIAA Journal,* Vol. 17, Aug. 1979, pp. 870-876.

[5] Thompson, J. F., Thames, F. C., and Mastin, C. W., "Automatic Numerical Generation of Body-Fitted Curvilinear Coordinate System for Field Containing Any Number of Arbitrary Two-Dimensional Bodies," *Journal of Computational Physics,* Vol. 15, No. 3, July 1974, pp. 299-319.

[6] Jameson, A. and Caughey, D. A., "A Finite Volume Method for Transonic Potential Flow Calculations," *Proceedings of the AIAA Third Computational Fluid Dynamics Conference,* Albuquerque, N. Mex., June 1977, pp. 35-54.

[7] Ashley, H. and Landahl, M., *Aerodynamics of Wings and Bodies,* Addison Wesley, Reading, Mass., 1965, p. 93.

[8] Varga, R. S., *Matrix Iterative Analysis,* Prentice-Hall, Englewood Cliffs, N. J., 1962, p. 196.

[9] Van Dine, C. P., "An Algorithm for the Optimization of Trajectories with Associated Parameters," *AIAA Journal,* Vol. 7, March 1969, pp. 400-405.

[10] Smith, S. M., "Discrete Frequency Sound Generation in Axial Flow Turbomachines," British Aeronautical Research Council, London, R&M 3709, 1971.

[11] Fung, Y. C., *An Introduction to the Theory of Aeroelasticity,* John Wiley & Sons, New York, 1955, pp. 166-168.